

Special Collection

In Situ Studies of the Formation of Tungsten and Niobium Oxide Nanoparticles: Towards Automated Analysis of Reaction Pathways from PDF Analysis using the Pearson Correlation Coefficient

Emil T. S. Kjær⁺,^[a] Olivia Aalling-Frederiksen⁺,^[a] Long Yang,^[b] Nancy K. Thomas,^[b] Mikkel Juelsholt,^[a] Simon J. L. Billinge,^{*,[b, c]} and Kirsten M. Ø. Jensen^{*,[a]}

Using Pair Distribution Function (PDF) analysis of in situ total scattering data, we investigate the formation of tungsten and niobium oxides in a simple solvothermal synthesis. We use Pearson Correlation Coefficient (PCC) analysis of the time resolved PDFs to both map the structural changes taking place throughout the synthesis and identify structural models for precursor and product through PCC-based structure mining. Our analysis first shows that ultra-small tungsten and niobium oxide nanoparticles form instantaneously upon heating, with sizes between 1.5 and 2 nm. We show that the main structural

motifs in the nanoparticles can be described with structures containing pentagonal columns, which is characteristic for many bulk tungsten and niobium oxides. We furthermore elucidate the structure of the precursor complex as clusters of octahedra with O- and Cl-ligands. The PCC based methodology automates the structure characterization and proves useful for analysis of large datasets of for example, time resolved X-ray scattering studies. The PCC is implemented in 'PDF in the cloud', a web platform for PDF analysis.

Introduction

While the intense focus on 'materials by design' over the last decades have led to mapping of structure/property relations in a range of new materials, we generally have limited knowledge on synthesis/structure relations, which slows down materials development.^[1] Material synthesis methods are to a large degree developed by extensive parameter studies based on trial-and-error experiments, and it is thus crucial to develop a deeper understanding of the mechanisms at play during material formation.^[1a] Here, in situ scattering studies can

provide new insight.^[2] Total scattering methods have been shown to be especially well-suited for studies of crystallization and deduction of reaction pathways in material formation. Analysis of total scattering data with for example, Pair Distribution Function (PDF) analysis allows structural information to be extracted from materials no matter if they are crystalline or not.^[3] This means that a synthesis process can be followed from ionic precursor clusters in solution, over amorphous intermediates to the final (nano)crystalline material,^[4] for example. New possibilities for advancing such experiments continually appear, and the amount of data that can be obtained from experiments at synchrotron beamlines continues to increase. While this provides new possibilities for time- and position-resolved experiments, analysis of the data becomes a bottleneck. There is thus a need for tools that can be used to automate and optimize the analysis of such data, such as the recently introduced structure-mining,^[5] cluster-mining^[6] and non-negative matrix factorization approaches.^[7]

We here study the formation of tungsten and niobium oxide nanoparticles during solvothermal synthesis in ethanol and isopropanol from metal chlorides.^[8] Both tungsten and niobium oxides have been studied intensely for a range of applications, including electrochromism and as battery cathodes.^[9] Their properties arise from their rich structural chemistry.^[10] If considering first tungsten oxides, a variety of crystal structures can form, which are all built from [WO₆]-octahedra with W mostly in oxidation state +4, +5, and +6. For example, several mixed oxides with oxidation states +5 and +6 exist, such as W₁₀O₂₉ and W₁₈O₄₉.^[10a] Their structures can be considered based on the ReO₃ structure, which contain octahedra with only corner-sharing geometry as illustrated in Figure 1a. Upon reduction, edge-sharing octahedra appear, which leads to the

[a] E. T. S. Kjær,⁺ O. Aalling-Frederiksen,⁺ Dr. M. Juelsholt, Dr. K. M. Ø. Jensen
 Department of Chemistry and Nano-Science Center
 University of Copenhagen
 2100 Copenhagen (Denmark)
 E-mail: kirsten@chem.ku.dk

[b] Dr. L. Yang, N. K. Thomas, Prof. S. J. L. Billinge
 Department of Applied Physics and Applied Mathematics
 Columbia University
 New York, NY 10027 (USA)
 E-mail: sb2896@columbia.edu

[c] Prof. S. J. L. Billinge
 Condensed Matter Physics and Materials Science Department
 Brookhaven National Laboratory
 Upton, NY 11973 (USA)

[*] These authors contributed equally to this work.

Supporting information for this article is available on the WWW under <https://doi.org/10.1002/cmtd.202200034>

Part of a Special Collection on In Situ and Operando Time-Resolved X-Ray and Neutron Diffraction Studies. Please visit chemistry-methods.org/collections to view all contributions.

© 2022 The Authors. Published by Wiley-VCH GmbH. This is an open access article under the terms of the Creative Commons Attribution Non-Commercial NoDerivs License, which permits use and distribution in any medium, provided the original work is properly cited, the use is non-commercial and no modifications or adaptations are made.

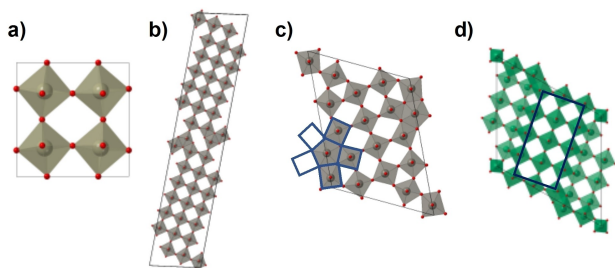


Figure 1. a) The ReO_3 structure with only corner-sharing $[\text{ReO}_6]$ octahedral. b) $\text{W}_{25}\text{O}_{73}$ containing shear planes of edge-sharing octahedra. c) $\text{W}_{18}\text{O}_{49}$ containing bipyramidal pentagonal columns of edge-sharing octahedra, as highlighted in blue. d) $\text{H-Nb}_2\text{O}_5$ which takes a Wadsley–Roth block type structure. The blocks, highlighted in blue, have the ReO_3 motif of 3×5 corner-sharing $[\text{NbO}_6]$ octahedra.

presence of Magnéli structures with shear planes ($\text{W}_{25}\text{O}_{73}$, Figure 1b), or bipyramidal pentagonal columns ($\text{W}_{18}\text{O}_{49}$, Figure 1c).^[11] The more reduced the compound is, the more shear planes or bipyramidal pentagonal columns are formed.^[10a] While these structures are well known in the bulk phase, they are difficult to distinguish in the case of nanoparticles, where the small size may also introduce structural changes which complicates structure analysis.^[12] Similar trends are seen in niobium oxides, which are also based on the ReO_3 structure. Here, oxides with mixed oxidation states (+5 and +6) are known to form Wadsley–Roth structures, as shown in Figure 1d for $\text{H-Nb}_2\text{O}_5$.^[13] The structural motifs of the Wadsley–Roth structures are likewise edge- and corner-sharing octahedra, which arrange in a block type structure. Blocks of corner-sharing octahedra (the ReO_3 motif) are separated by slaps of edge-sharing octahedra, and the many different reported structures differ from the block size and block arrangement.^[14]

We here investigate the tungsten and niobium oxide synthesis varying the reaction temperature and solvent (ethanol and isopropanol). To automate the data analysis and understand correlations and differences between datasets, we introduce simple tools building on the use of Pearson Correlation Coefficient (PCC) analysis. The PCC is a measure of how linearly correlated two datasets are, and in this case how similar two PDFs are. It is defined as Equation (1):^[15]

$$r = \frac{1}{1-n} \sum_{i=0}^n \left(\frac{X_i - \bar{X}}{\sigma_x} \right) \left(\frac{Y_i - \bar{Y}}{\sigma_y} \right) \quad (1)$$

Here, X and Y are the two datasets being compared, that is, here two PDFs. The sum goes over points of each PDF. \bar{X} and \bar{Y} are the mean values and σ_x and σ_y are the standard deviations of X and Y, respectively. The PCC can take any value between -1 and 1 depending on the correlation. Having a PCC equal to 1 corresponds to a perfect linear correlation, while a PCC of -1 indicates opposite behavior between the two functions. This correlation measure is scale invariant, hence only taking peak positions and widths into account. It is thus a quick and simple way of comparing PDFs or other datasets.^[15–16] We first use the PCC of measured PDFs to gain an overview of the time resolved in situ data and identify structural changes taking place in the

synthesis process.^[17] We also use the PCC for automated structure-mining, where all relevant oxides present in structural databases are compared to experimental PDFs using the PCC. A similar approach has been used for organic molecules where a number of compounds were compared to an experimental PDF.^[18] Our automated PCC analysis, taking advantage of database mining, allows us to quickly identify structures which can describe the experimental data from the small nanoparticles of tungsten and niobium oxides, which we compare and use for further structure analysis. We also use PCC analysis of simulated PDFs from tungsten and niobium oxides to identify the limitations in PDF modelling based on bulk structures for analysis of ultrasmall nanoparticles of complex materials with a high degree of defects and disorder.

Our results reveal the formation of ultrasmall tungsten and niobium oxide nanoparticles, which have pentagonal columns as the main structural motif. The particles form directly from $[\text{MO}_x\text{Cl}_y]$ (M: W or Nb) complexes, and only limited structural changes are seen after the instantaneous nanoparticle nucleation when starting the experiment. At the same time, we highlight how the PCC tools can be applied for analysis of time resolved datasets. PCC analysis is implemented in ‘PDF in the cloud’ (PDFit),^[19] which is a web platform hosting a series of analysis applications for user-uploaded PDF data.

Experimental Methods

Nanoparticle synthesis and in situ experiments

Tungsten oxide nanoparticles were synthesized using two different solvents but the same precursor compound. WCl_6 ($\geq 99.99\%$, Sigma–Aldrich) was dissolved in 15 mL of isopropanol or ethanol to reach a 0.3 M tungsten concentration. The solution was then vigorously stirred until the powder was completely dissolved and the solution turned dark blue. Niobium oxide nanoparticles were synthesized in a similar manner. NbCl_5 (99%, Sigma–Aldrich) was dissolved in either isopropanol or ethanol to reach a niobium concentration of 0.6 M. Both precursor solutions were prepared at room temperature and in air.

The synthesis was done in our custom-made reaction cell for in situ X-ray studies of solvothermal synthesis, which is similar in design to that previously described by Becker et al.^[20] The precursor suspension was injected into a fused silica tube with 0.7 mm inner diameter and 0.09 mm wall thickness. The pressure during reaction was kept stable at 100 bar throughout the experiment using an HPLC pump. A heat gun was used to heat the capillary containing the precursor. Initially, no heat was applied to allow for data collection from the precursor. The heat was turned on approximately 30 seconds after data collection had been initialized. The exposure time for each frame in the dataset was 5 seconds. Experiments were done at 120 °C, 150 °C, 200 °C, 255 °C, 300 °C and 310 °C.

The in situ total scattering experiments were done at beamline P02.1, PETRA III, DESY in Germany with a wavelength of 0.207 Å and a detector distance of 210 mm. A Perkin Elmer XRD1621 area detector with a pixel size of 0.2×0.2 mm was used. The Rapid Acquisition Pair Distribution Function (RA-PDF) setup was used for all experiments.^[21]

Data analysis

The collected 2D data were integrated using PyFAI,^[22] and the total scattering data were Fourier Transformed to obtain PDFs using PDFgetX3.^[23] Before the Fourier transformation, the background scattering signal from the fused silica capillary and the pure solvent at the appropriate temperature and pressure were subtracted. The PDFs were analyzed using the PCC in SciPy,^[24] and they were compared to structures obtained from the Crystallographic Open Database (COD)^[25] and Inorganic Crystal Structure Database (ICSD).^[26] PDF modelling was done using DiffPy-CMI^[27] and PDFgui.^[28] PCC analysis is implemented in PDFfitc.^[29]

Results and Discussion

Formation of tungsten oxide nanoparticles: Overview of reaction process from PCC analysis

To reveal the formation pathway of tungsten oxide, eight in situ total scattering experiments were conducted, investigating the influence of the alcohol (ethanol vs. isopropanol) and reaction temperature (between 120 and 310 °C). First, we investigate the synthesis of tungsten oxide from tungsten hexachloride in isopropanol at 310 °C. Figure 2a shows the contour plot of total scattering structure functions ($F(Q)$) obtained from the total scattering data. The corresponding contour plot of the reduced PDFs, $G(r)$, is presented in Figure 2b. The PDFs obtained after 5 minutes of heating for each experiment are shown in Figure 2c. Similar representations of the data from other experiments can be found in section A in the Supporting Information.

The reaction is initiated by heating at time $t=0$ s. Before initiating the experiment, we observe no Bragg peaks in the Q -space data, Figure 2a. When considering the corresponding PDFs, only short-range order is observed. However, as soon as the heating is initiated, the signal from the precursor disappears and nanocrystalline particles form. In the Q -space data, this is seen from broad features indicating the formation of small nanoparticles. The r -space PDFs (Figure 2b–c) also show limited long-range order, with the PDFs showing a maximum crystalline domain size of approximately 15–20 Å, Figure 2c. The transformation from precursor complex to nanocrystalline particles appears to happen faster than the time resolution of the in situ PDF experiment of 5 s, hence within one frame.

Before further structural analyses of the product and precursor phases, we apply PCC analysis to identify possible changes throughout the measurements. Figure 2d–f show PCC matrices obtained when comparing all PDFs in the in situ dataset from tungsten oxide formation in isopropanol at 310 °C. The matrices are calculated over 2 different r -ranges, 1.5–15 Å (Figure 2d–e) and 1.5–7.5 Å (Figure 2f). The PCC matrices clearly show that the formation of the nanocrystalline tungsten oxide takes place directly from the precursor structure, as no intermediate structure is observed in either of the two r -ranges investigated. The correlation between frames obtained before heating is initiated is almost 1 in all cases, indicating that the precursor structure is stable. The same is observed in the frames obtained after heating, where the PCC values are also close to 1 throughout the experiment. This illustrates that no significant changes of the nanoparticles structure take place after

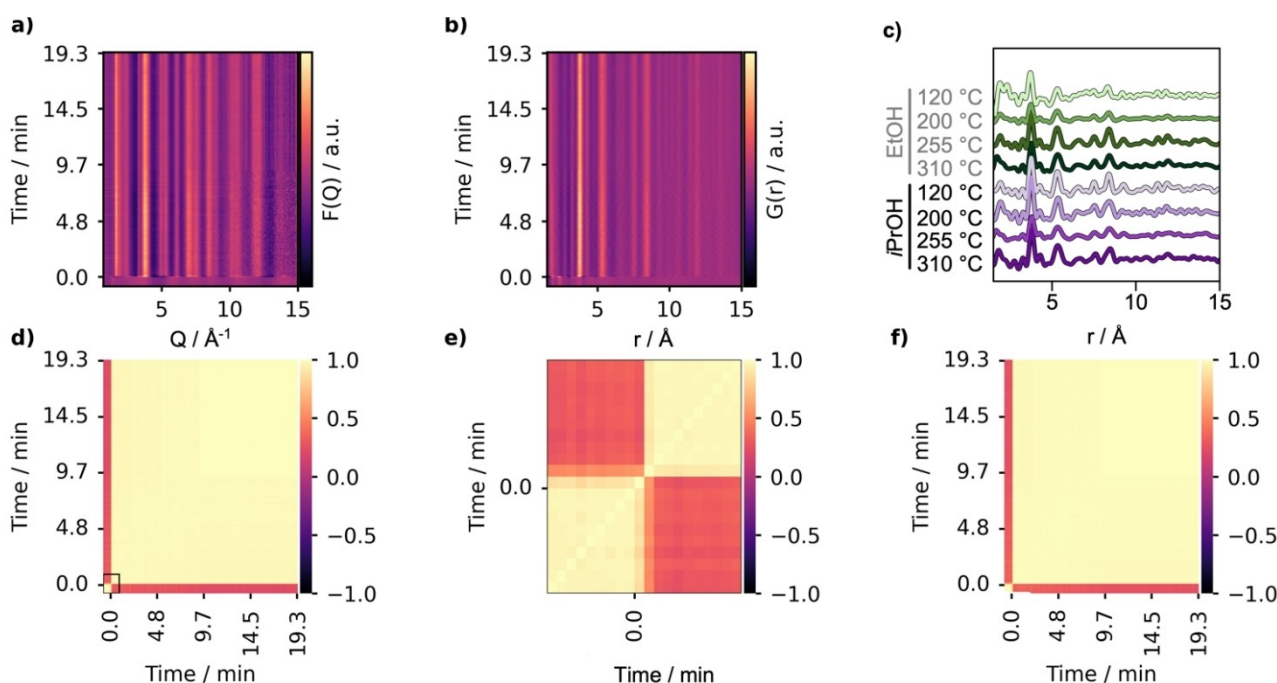


Figure 2. Time resolved PDFs obtained from the synthesis of tungsten oxide in isopropanol at 310 °C. a) Contour plot of reduced structure functions $F(Q)$. b) Contour plot of the corresponding PDFs. c) PDF of the product phases after 5 minutes, comparing all tungsten oxide experiments. d–e) PCC matrices between the time-resolved PDFs using the r -range of 0–15 Å. f) Correlation matrices between the time-resolved PDFs using the r -range of 0–7.5 Å. The color bar goes from -1 to 1 where black is -1 and yellow is 1 .

nucleation. The low correlation between precursor and product (Figure 2e) indicates only limited structural relation. Similar results are observed from the PCC matrices obtained from the remaining in situ datasets as shown in Figure S1–S7 in Supporting Information. They all show similar trends, except for the experiment done in ethanol at 120 °C, where few structural changes are seen upon heating as discussed further below.

Structure identification using PCC-based structure mining

From the correlation matrices, two distinct stages of the reaction can be identified: precursor and product. We first characterize the nanoparticle product. The PDFs obtained from all tungsten oxide product phases (as observed after 5 min of reaction) are plotted in Figure 2c. Tungsten oxides exist in numerous polymorphs, and as we have previously shown, nanostructured materials may take structures different from those known from the bulk.^[12,30] A bottleneck in structure analysis of such compounds is thus identifying a suitable model for structure refinement. This has been addressed by the structureMining app at the PDFfit.org website^[19] where candidate structural models are provided after uploading a PDF and some compositional information. Here we show that similar behavior can be obtained through the application of the PCC to optimize and automate this analysis. By automatically calculating the correlation between experimental and simulated PDFs, vast numbers of structures can be tested within a short period of time. For this analysis we use models from two structure databases, the COD and the ICSD. All structures containing both W and O were used, providing a total structure list of 5634 structures, from which PDFs were simulated. The five most promising structures for the last PDF extracted from the dataset are shown in Table 1. The workflow is described in greater detail in section B in the Supporting Information. In the future we will explore adding this capability to PDFfit.org to speed up the structureMining process.

The PDF fits using the five best candidate structures are shown in Figure 3a–f and a further description of the fit strategy can be found in section C in the Supporting Information. The crystal structures used in the refinements are illustrated next to the corresponding fit in Figure 3. The first W–O PDF peak at 1.8 Å is excluded from the refinements as the broad and asymmetric profile of the W–O peak (Figure 2c) challenges the analysis of the complete *r*-range. The shape most likely relates to oxygen disorder in the tungsten oxide nanomaterial, which

Table 1. List of the five most promising structure candidates for the PDF obtained for the synthesis in isopropanol at 310 °C obtained from the 5634 structures analyzed. The structures are sorted from highest to lowest PCC value. The R_{wp} values have been obtained from PDF fitting.

Structure	PCC	R_{wp} [%]
W_5O_{14}	0.89	26.3
$W_{18}O_{49}$	0.86	27.9
$W_{32}O_{84}$	0.82	31.7
$W_{17}O_{47}$	0.79	38.1
$W_{25}O_{73}$	0.77	37.0

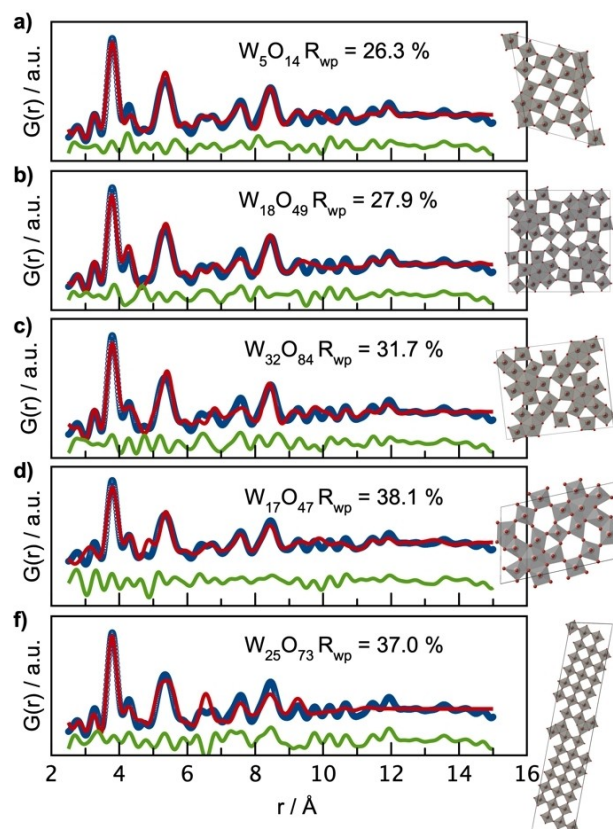


Figure 3. Refinements of the PDF from WO nanoparticles synthesized in isopropanol at 310 °C, using the five best candidate structures obtained from the PCC analysis. a) W_5O_{14} , b) $W_{18}O_{49}$, c) $W_{32}O_{84}$, d) $W_{17}O_{47}$, e) $W_{25}O_{73}$. Blue dots represent the experimental PDFs, the red line the calculated PDFs and green line the difference curves between the two.

we have observed previously in formation studies of nanosized tungsten and niobium oxides.^[4a,12c]

The candidates extracted from the PCC analysis are all non-stoichiometric oxides, which contain bipyramidal pentagonal columns, or the Magnéli structural motif with shear planes, as represented in Figure 1c and b respectively. Figure 3 shows that the best fits are obtained from the crystal structures with bipyramidal pentagonal columns, that is W_5O_{14} and $W_{18}O_{49}$, which both contain tungsten in oxidation state +5 and +6. The data thus indicate a partly reduction of the metal by the isopropanol during the reaction from WCl_6 . Tungsten oxide nanoparticles synthesized using a similar reaction route, although in benzyl alcohol,^[8a,31] have previously been reported to take the $W_{18}O_{49}$ structure based on PXRD analysis.^[32] In our list (Table 1) $W_{18}O_{49}$ appears as the 2nd candidate, and shows a high correlation value and a relatively good fit quality for nanocrystalline materials with a R_{wp} -value of 27.9%. However, we also notice that all five structures can describe the most characteristic features of the experimental PDF (Figure 3), and therefore it is challenging to make finite conclusions from these unique structures.

To quantify the issue, and to put a numerical value on how similar the proposed structures are, we again use the PCC. PCC analysis between the PDFs of the seven best structures were

performed, and the obtained correlation matrices are shown in Figure 4. PDFs were simulated for each of the model structures (simulation parameters in section D in the Supporting Information), and PCC matrices were computed. PCC matrices were constructed for three separate cases: 1) Calculated with 'small' ADP-values of 0.003 \AA^2 and structural parameters as reported in CIFs, 2) with larger ADP-values of 0.01 \AA^2 and structural parameters as reported in CIFs, and 3) refined structural parameters and ADP values (Figure 4a–c). Note that high refined ADP values may not only relate to thermal vibrations but can cover different kinds of disorder in the structure, and high values are often obtained in nanomaterial analysis.

From Figure 4a, we observe that when low ADP values are used, it is possible to distinguish between the structure candidates based on the PCC-values (0.60–0.80). However, when the ADP values are increased to more physical values, and especially when using the refined structural parameters against the data set, it becomes virtually impossible to distinguish between the structures containing the same motifs. Only the PDF of the WO_3 structure seems to differ slightly from all other structures. The discrepancies can be explained as the bulk WO_3 structure only contain corner-sharing and no edge-sharing $[\text{WO}_6]$ octahedra.

These correlations are crucial to consider when identifying the structure from a PDF, or any other dataset. While PDF is generally a strong tool for structure analysis of nanomaterials, the large similarity between the models from these bulk materials makes it difficult to assign a specific structure to the very small nanoparticles synthesized here. We also note that at least one dimension in the unit cell for the $\text{W}_{18}\text{O}_{49}$ and W_5O_{14} structures (as well as other WO_x structures) is larger or of the same size as the particles that form in the synthesis (18 \AA), therefore it may not be meaningful to describe these with crystal structures known from bulk materials. Instead, we interpret the structure mining results as the sample contains a structural motif of pentagonal columns.

Structure dependence of synthesis parameters

Having established the structure of the final product in the synthesis done at 310°C in isopropanol above, we can now compare to the results of syntheses conducted under other conditions. Figure 2c shows the final PDFs obtained for all experiments. A PCC matrix comparing them is shown in Figure 5a. We generally see high correlation values, confirming the high structural similarity between the products. The average PCC is 0.87, and only the PDF from the reaction in ethanol heated at 120°C gives slightly lower PCC values. As shown from the contour plot related to this experiment (Figure S1 in the Supporting Information), no significant changes take place from precursor to final material in this experiment. It appears that some nanoparticles have appeared already at the precursor stage, but also that some of the precursor clusters (discussed below) remain during the in situ experiment, which gives a lower correlation to other product PDFs.

PCC structure mining on the product PDFs for all experiments are given in section E in the Supporting Information (Tables S4–S10), and the results show that the W_5O_{14} structure model can describe the resulting PDF of all experiments, except for the experiment with ethanol at 120°C . We therefore performed sequential refinement using W_5O_{14} as the structural starting model. Examples of refinements and resulting values are given in section E and F in the Supporting Information. Figures 5b–d highlight how crystallite size, scale, and fit-quality (R_{wp}) evolve throughout the seven experiments. The results show that no major changes take place over time in all seven cases. Considering the nanocrystallite size in Figure 5b, all experiments result in particles between 1.5 and 2 nm, with no significant growth within the time-range of the experiment. We do not observe a clear size effect of synthesis temperature, but synthesis in ethanol appears to result in slightly larger particles than isopropanol. Both the scale factor (Figure 5c) and the fit-quality (Figure 5d) also seem to be reasonably stable throughout the time scale of all experiments. A stable scale factor points towards no additional particle formation with time,

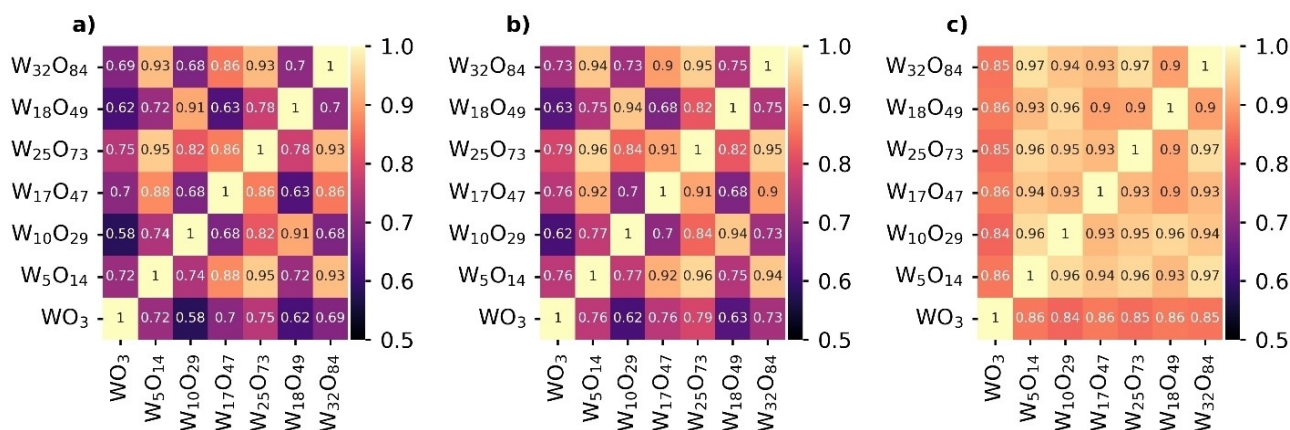


Figure 4. PCC matrices of the seven best structural predictions for WO_x synthesized in isopropanol at 310°C . a) Shows the PCC values for simulated PDFs using a $U_{\text{iso}} = 0.003 \text{ \AA}^2$ and b) with a $U_{\text{iso}} = 0.01 \text{ \AA}^2$ (The remaining simulation parameters are shown in section B in the Supporting Information). c) For comparison the PCC matrix of the fitted structures is presented. All calculated from 2.5 to 15 Å. Note that the PCC colourbar goes from 0.5 to 1 to increase contrast. The average PCC value for each matrix is a) 0.75, b) 0.80 and c) 0.91.

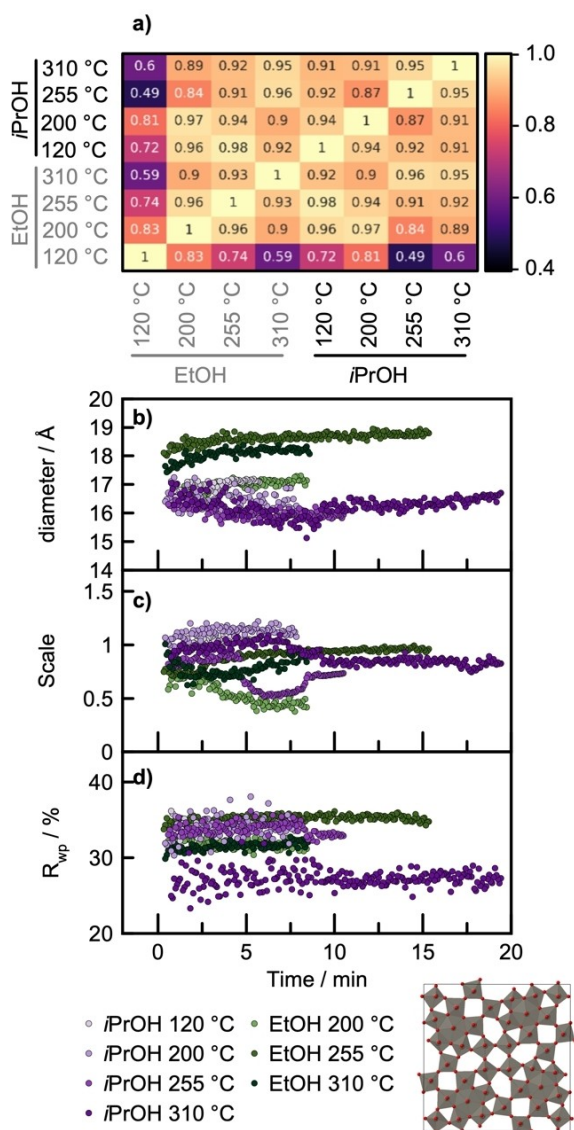


Figure 5. a) PCC matrix showing the correlation between the last frame of each of the 8 WO_x experiments in the data range 1.5–15 Å with a mean PCC of 0.87. Note that the color range is set to 0.4 to 1 to highlight differences. b–d) Results from sequential refinements with W_5O_{14} showing that no significant changes are observed over the time ranges of the experiments for crystallite diameter (b), scale (c) and R_{wp} (d).

whereas the fit-quality again confirms that there are no significant structural changes, and that the same structural model can describe the data throughout the whole time-range. Small changes in the scale (as that observed from the drop in the scale in isopropanol at 255 °C Figure 5c) most likely relate to particles moving in and out of the X-ray beam during the experiment.

Figures S15 in section F in the Supporting Information shows the additional structural parameters from the sequential refinements plotted over time, confirming that also cell-parameters are unaffected over time. Additional sequential refinements were performed and are also shown in section F in the Supporting Information. Here, eight individual structure models, extracted from the structure-mining approach, are

refined towards the eight individual experiments. It shows how all structures result in similar trends as just described above for the W_5O_{14} structure, and again supports the finding that the structures are hardly distinguishable and all able to describe the PDFs of the ultra-small particles synthesized here.

Precursor structure

We now investigate the structure of the precursor material. Figure 6a shows the eight PDFs obtained for the tungsten oxide precursors, which are in all cases WCl_6 dissolved in either ethanol or isopropanol at room temperature. Note that the temperatures related to the PDFs in Figure 6a relate to the reaction temperature used later in the experiment. The initial PCC analysis shown in Figure 2e showed very low correlation between the precursor and the product PDFs, which shows that the precursor structure is not related to tungsten oxide structures. As also reflected in PCC matrix in Figure 6b, we see

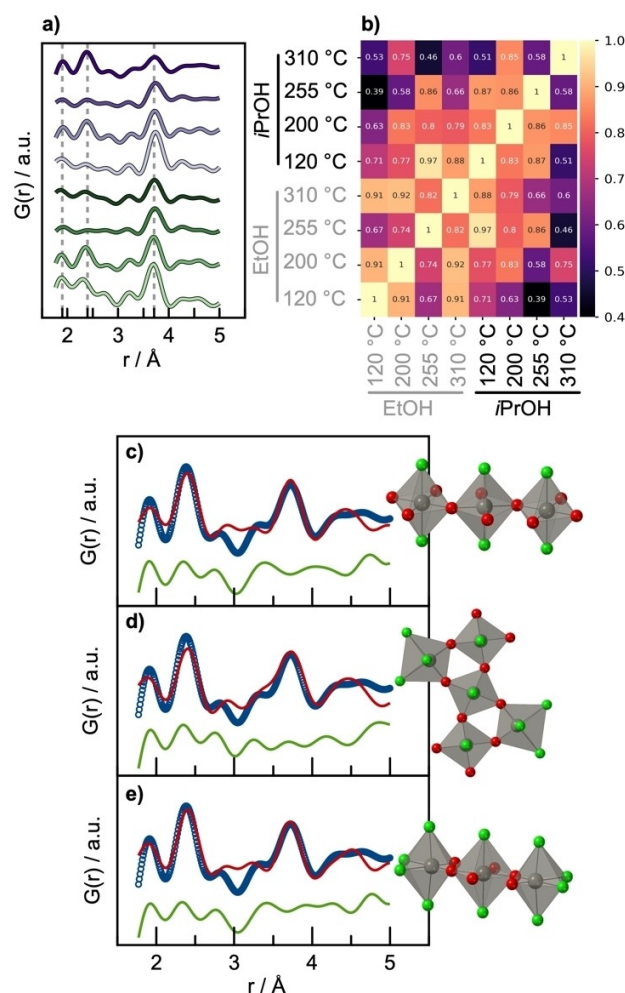


Figure 6. a) PDFs from precursor of each of the eight WO_x experiments. b) PCC showing correlations between the PDFs shown in a. c–d) Fits to the precursor for the WO_x synthesis in isopropanol at 310 °C, using a chain of corner-sharing $[WO_2Cl_4]$ octahedra I, a cluster of five corner-sharing $[WO_{6-x}Cl_x]$ octahedral (d) and a chain of corner-sharing $[WO_{6-x}Cl_x]$ octahedral (e).

fairly large differences between the precursor PDFs, even for those prepared in the same solvent. In all cases, a clear peak in precursor PDF is seen at ca. 2.4 Å, and this peak has a shoulder at 1.9 Å (highlighted with dotted lines in Figure 6b). Considering the precursor material, the peak at 2.4 Å is likely to arise from a W–Cl pair, while the peak at 1.9 Å agree with the W–O distance.^[33] However, a PDF peak is also seen at 3.8 Å, corresponding to the W–W distance between corner-sharing octahedra.

To automate the analysis of the precursor structure, we again use a database search and PCC analysis to identify structural motifs. To build up a suitable database for the precursor analysis, we included compounds containing tungsten, oxygen, chlorine, as well as molybdenum, tantalum, and niobium, as it is well known that these metal oxide compounds share some of the same structure and cluster chemistry^[9a,13,34] With these search criteria, we obtained a database with more than 15 000 structures. We then performed a PCC analysis using these systems against the precursor PDF from the experiment in isopropanol at 310 °C, only including the *r*-range from 0 Å to 7.5 Å. The best structural candidates are listed in section G in the Supporting Information, along with their PCC values. Note that these values are in general slightly lower than those obtained in the PCC analysis of the tungsten oxide nanoparticles. This can be explained by the nature of the precursor: The precursor structure is a small cluster, and we here using crystal structures to describe the very limited structural order in the PDF.

When considering the structures with the highest PCC compared to the experimental PDF, they are generally metal oxides and oxychlorides, where metals are octahedrally coordinated, linked through oxygen and coordinated to chlorine. To develop a structural model for the precursor, we cut out structural motifs from the best structure candidates, and fit them to the PDF using the Debye Scattering Equation.^[35] Figure 6c–e shows the fits of the three best fitting structures, obtained as cut-outs from crystal structure of Ta₂Cl₇N₆H₁₅ (the crystal structure is shown in Figure S24) where N was replaced for O, H removed, and Ta replaced with W. Since we are fitting clusters to a very narrow *r*-range the number of free parameters during this refinement was kept to a minimum. Only the scale factor and expansion/contraction parameters along the *x*, *y* and *z* axes were refined to avoid overfitting. These cluster structures generally give a good fit to the PDF, describing both the W–O peak (1.9 Å), the W–Cl peak (2.4 Å), and the peak at ca. 3.8 Å, which arises from W–W pairs. As seen from Figure 6c–e, we cannot determine a unique structure model for the cluster, and the PDF is not sensitive towards, for example, the exact number of atoms and their arrangement. However, the precursor can be described as a polymeric complex of corner-sharing [WCl_{6-x}O_x] octahedra. The formation of a W–O–W and partly substitution of Cl when dissolving WCl₆ in an alcohol has also been observed using EXAFS by Olliges-Stadler et al.^[36]

When comparing the precursor PDFs obtained for the eight different syntheses (Figure 6a), we observe some discrepancies, most clearly seen from the differences in the intensity ratio for the W–O, W–Cl, and W–W peaks, however, there is no system-

atic trend distinguishing, for example, the samples prepared in ethanol and isopropanol. We assign these differences to the experimental conditions used when preparing the samples for in situ experiments. Some of the precursor solutions had aged for 1–3 h before the in situ experiments were performed in the fused silica reactor cell. As the experiments were done in air, it is highly likely that moisture have affected the state of the precursor complex, as WCl₆ readily hydrolyzes to WOCl₄ and WO₂Cl₂ which might cause structural differences upon dissolution.^[36] Furthermore, the solvent, especially ethanol, most likely contains some amount of water.

Refinements of the precursor PDFs from the seven other experiments are shown in section G Figure S25 in the Supporting Information showing that the same models can describe the precursor structure of the different experiments. We thus conclude that while structural differences are seen, the precursors all contain the same motifs. A formation mechanism is suggested below in section 3.6.

Formation of niobium oxide

To further explore the reaction and establish use of the PCC methodology for other systems, we also conducted experiments on the formation of niobium oxide nanoparticles in ethanol and isopropanol. We first consider the experiment at 300 °C isopropanol. Figure 7a shows the contour plot of the PDFs. Similar plots of data from other experiments (isopropanol 150 °C and ethanol 150 °C and 300 °C) are shown in section H in the Supporting Information.

A PCC analysis of the in situ data is shown in Figure 7b, and a zoom-in of the PCC in the precursor to final product transition in Figure 7c. Here, we observe how the reaction process is very similar to that observed in the case of tungsten oxide, where only two distinct stages are present – a precursor and a nanocrystalline stage.

We now use the PCC-based structure mining to investigate the structure of the final product. From the databases we extract structures containing Nb or W and O, which gives in total 7693 for further analysis. Table 2 presents the four most promising structures, the corresponding PCC values, and the fit-quality (*R*_{wp}-values). The proposed PCC structures for the remaining three niobium oxide experiments are shown in section I in the Supporting Information. Surprisingly, all the best structures are tungsten oxides, and not the bulk niobium oxide structure one could expect. Figure 7d shows refinements using

Table 2. From the 7693 structures analyzed the four most promising structure candidates for the PDF obtained for the synthesis in isopropanol at 300 °C are shown. The structures are sorted after the PCC ranging from highest to lowest. Additionally, the *R*_{wp}-values have been determined after fitting.

Structure	PCC	<i>R</i> _{wp} [%]
W ₁₈ O ₄₉	0.80	47.4
W ₅ O ₁₄	0.74	47.6
W ₁₇ O ₄₇	0.73	51.0
W ₃ O ₈	0.70	52.0

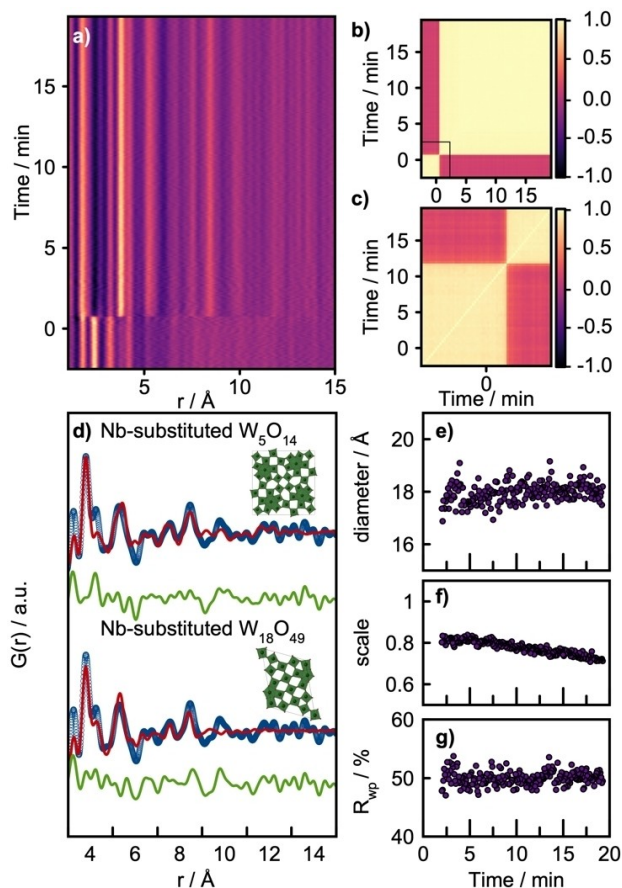


Figure 7. a) Contour plot of the PDFs showing the formation of niobium oxide. b-c) PCC throughout the experiment, proving that the transition from precursor to final product is happening fast after applying heat. d) Refinement using two of the most promising structure found from PCC analysis. From sequential refinement using the Nb-substituted W_5O_{14} structure the change over time of the e) diameter, f) scale factor and g) R_{wp} -value. No significant changes are observed over time.

$W_{18}O_{49}$ and W_5O_{14} as the structural starting model respectively. In all refinements, W are replaced for Nb, and refinement parameters and additional fits are shown in section J in the Supporting Information. Both structures provide a good agreement with the experimental data. From additional sequential refinements, using the W_5O_{14} structural starting model, we show how the structural parameters, size, scale and R_{wp} (Figure 8e–g) are all stable throughout the time-range of the experiment.

Results from sequential refinements using the two most promising structures (W_5O_{14} and $W_{18}O_{49}$, with W substituted for Nb) are plotted for all four experiments in section K in the Supporting Information.

To investigate why the PCC analysis finds tungsten-based materials rather than niobium-based structures, we conducted PCC analysis between the five most reported niobium structures ($T-Nb_2O_5$, $Nb_{22}O_{54}$, $H-Nb_2O_5$, $Nb_{12}O_{29}$ and $M-Nb_2O_5$),^[14] together with the two most promising structures found in the PCC analysis ($W_{18}O_{49}$ and W_5O_{14}) to elucidate the similarities and differences of the structures. The PCC matrices are shown in section L in the Supporting Information. The results show that

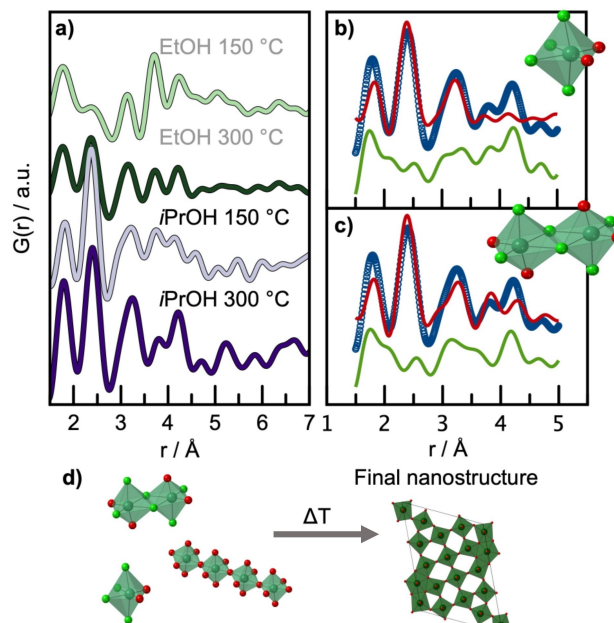


Figure 8. a) Comparison of the different precursors for the four experiments. Refinements on the precursor collected for the experiment in isopropanol heated to 300 °C b) using a single $[NbCl_{1-x}O_x]$ octahedra. c) Refinement using a cluster of edge-sharing $[NbCl_{1-x}O_x]$ octahedra.

with low U_{iso} values for both the metal and oxygen sites (0.003 \AA^2) we can distinguish between the tungsten and niobium structures based on the PCC-values. Here, especially $T-Nb_2O_5$ and $M-Nb_2O_5$ differ significantly from the others with PCC-values around 0.3. However, when instead comparing the PDFs of the seven phases with refined U_{iso} values, we see that PDFs are highly similar. They are all able to describe the same data and differentiating between them is challenging. This again highlights that caution should be taken when analyzing the structure of such small nanoparticles with complex structures, and that the main conclusion is that the best structures suggested by the algorithm all contain pentagonal columns. Refinements using both tungsten and niobium oxide structures are found in section J in Supporting Information.

We now investigate the precursor structure of the niobium synthesis. All precursor PDFs originate from the $NbCl_5$ dissolved in either ethanol or isopropanol at room temperature. Figure 8a shows the PDFs compared for the four experiments, where the temperature relates to the later reaction conditions. It is observed that all precursor PDFs have peaks at 1.8 Å and 2.4 Å with differing ratios. The precursor for the ethanol experiment at 150 °C also has a sharp PDF peak around 3.8 Å, which we also observed for the tungsten precursors in Figure 6. As the peak most likely originate from a metal-metal correlation, it points towards an extended structural order for only this niobium oxide precursor. As discussed for tungsten oxide, we relate these differences in the precursor structures to, for example, ageing and moisture which affects the state of the precursor complex, as the experiments were conducted in air. We have previously observed similar effects for $NbCl_5$ in benzyl alcohol.^[12c]

Using a similar approach as for the tungsten system, we investigate the precursor structure to find a structural motif and extract from already reported bulk crystal structures. Again, a database of more than 15 000 structures was used including niobium, tungsten, molybdenum, and tantalum structures. For the isopropanol 300 °C experiment, we found that the precursor structure can be described by an Nb substituted $[\text{TaCl}_4\text{O}_2]$ octahedra, which our algorithm extracted from the crystal structure of $\text{TaCl}_3\text{NO}_2\text{H}_{39}\text{C}_{29}$, as illustrated in Figure S33 in the Supporting Information. Lists of the most promising candidates found from the analysis are presented in the section M in Supporting Information. The refinement using the structural motif of a single $[\text{NbCl}_4\text{O}_2]$ octahedra is shown in Figure 8b. However, a larger cluster of edge-sharing $[\text{NbCl}_{6-x}\text{O}_x]$ octahedra can also describe the data (Figure 8c). The PDF peak at 3.1 Å can potentially be described both as a ligand-ligand distance in the octahedra, as well as a Nb–Nb edge-sharing octahedra distance. Most likely, the precursor contains clusters of several different sizes with $[\text{NbCl}_{6-x}\text{O}_x]$ as the main motif. Similar results were obtained for the three additional experiments as shown in section M in Supporting Information.

Formation mechanism

Based on the PCC PDF studies described above we suggest a formation mechanism of tungsten and niobium oxide from the metal chloride in ethanol or isopropanol, illustrated in Figure 9. We have shown that the two systems follow a similar pathway: When dissolving MCl_6 ($\text{M}=\text{W}, \text{Nb}$) in either of the alcohols used here, Cl-ligands are partly but rapidly exchanged for oxygen, resulting in a metal oxychloride complex. Since the X-ray PDFs are not sensitive to hydrogen, we are not able to deduce whether the oxygen coordination is O^{2-} , OH^- or an alkoxide. The oxygen donor is expected to be the alcohol, as suggested by Niederberger et al., resulting in the reaction products of chlorides or ethers of the corresponding alcohol.^[8c,36] However, since the syntheses were conducted in air, we cannot exclude that the alcohols are contaminated by water. Water would consequently be able to take part in the hydrolysis of the chloride precursor.^[8c] As M–M pairs are already seen at the precursor stage, we suggest that condensation of $[\text{MCl}_{6-x}\text{O}_x]$ octahedra to form polymeric structures with corner-sharing octahedra take place very rapidly after exchange of Cl-ligands. The transition from the polymeric $[\text{MCl}_{6-x}\text{O}_x]_y$ complex to the

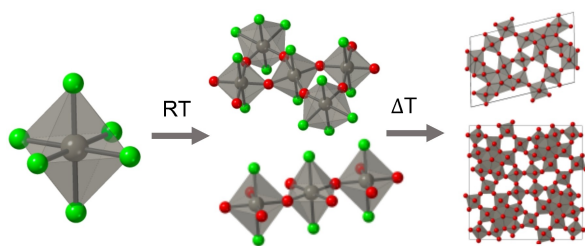


Figure 9. Proposed formation pathway, going from MCl_6 to $[\text{MCl}_{1-x}\text{O}_x]$ ($\text{M}=\text{W}, \text{Nb}$) clusters to metal oxide nanoparticles with pentagonal columns.

final metal oxide nanoparticles happens in less than 5 s upon heating.

The formed nanocrystalline material takes a metal oxide structure with the structural motif of pentagonal columns, and the differences in the precursor structure discussed above do not seem to have any influence on the final product. Slightly larger tungsten oxide particles are observed from reactions in ethanol compared to isopropanol for tungsten oxide. Due to the nature of the alcohols we would expect the ethanol to react slower, however, with the alcohols being contaminated by water, it might consequently influence the rate of reaction and thereby the final size of the formed nanoparticles.

Conclusion

Using simple tools based on the Pearson Correlation Coefficient (PCC), we have studied the formation of tungsten and niobium oxide from in situ total scattering data and PDF analysis. We have shown that the methodology is useful to obtain an overview over large datasets and for searching through thousands of CIFs, which can help to automate and optimize the data analysis. Our analysis shows that PCC analysis is useful for identifying structural motifs in disordered and nanostructured materials, where a single crystal structure may not be suitable for describing the material. Instead, specific motifs can be identified by considering the ranking of structures in the PCC list and comparing these against the data. It also highlights how it is crucial to be aware of the limitations of using well-ordered bulk structures for modelling. A PCC tool for comparing datasets, as presented in the article, is available in the similarityMapping software app at PDFitc.org.^[19] Users may upload a set of PDFs and the app will return back the Pearson correlation matrix for inspection without having to write any code.

Using these PCC tools we have been able to elucidate the formation mechanism for tungsten and niobium oxides in ethanol and isopropanol from metal chloride precursors. Upon dissolution, chloride ligands are replaced by oxygen from the solvent, and the resulting complexes of $[\text{MCl}_{6-x}\text{O}_x]$ octahedra ($\text{M}=\text{W}, \text{Nb}$) assemble to polymeric clusters. Initiation of heating leads to immediate nucleation of metal oxide nanoparticles. Both the tungsten and niobium oxides formed can be described using models from bulk crystal structures built up from bipyramidal pentagonal columns, such as the W_5O_{14} and $\text{W}_{18}\text{O}_{49}$ structures.

While the in situ total scattering datasets here are fairly simple, the PCC tools presented can easily be extended to much larger studies, where it is crucial to quickly establish an overview of, for example, structural differences and occurrence of different phases.

Acknowledgements

This work is part of a project that has received funding from the European Research Council (ERC) under the European Union's

Horizon 2020 Research and Innovation Programme (grant agreement No. 804066). We are grateful to the Villum Foundation for financial support through a Villum Young Investigator grant (VKR00015416). Funding from the Danish Ministry of Higher Education and Science through the SMART Lighthouse is gratefully acknowledged.

We furthermore thank DANSCATT (supported by the Danish Agency for Science and Higher Education) for support. We acknowledge DESY (Hamburg, Germany), a member of the Helmholtz Association HGF, for the provision of experimental facilities. Parts of this research were carried out at beamline P02.1 at Petralim and we would like to thank Martin Etter for assistance in using the beamline. S.J.L.B. was supported by the U.S. National Science Foundation through grant DMREF-1922234.

Conflict of Interest

The authors declare no conflict of interest.

Data Availability Statement

The data that support the findings of this study are available from the corresponding author upon reasonable request.

Keywords: automated data analysis · in situ · nanoparticles · Pearson correlation · total scattering pair distribution function analysis

- [1] a) L. Soderholm, J. Mitchell, *APL Mater.* **2016**, *4*, 053212; b) B. G. Sumpter, R. K. Vasudevan, T. Potok, S. V. Kalinin, *npj Comput. Mater.* **2015**, *1*, 15008.
- [2] a) K. M. Ø Jensen, M. Christensen, P. Juhas, C. Tyrsted, E. D. Bøjesen, N. Lock, S. J. Billinge, B. B. Iversen, *J. Am. Chem. Soc.* **2012**, *134*, 6785–6792; b) K. M. Ø Jensen, C. Tyrsted, M. Bremholm, B. B. Iversen, *ChemSusChem* **2014**, *7*, 1594–1611; c) C. Tyrsted, K. M. Ø Jensen, E. D. Bøjesen, N. Lock, M. Christensen, S. J. Billinge, B. B. Iversen, *Angew. Chem. Int. Ed.* **2012**, *51*, 9030–9033; *Angew. Chem.* **2012**, *124*, 9164–9167; d) E. Bøjesen, B. Iversen, *CrystEngComm* **2016**, *18*, 8332–8353.
- [3] a) S. J. L. Billinge, M. G. Kanatzidis, *Chem. Commun.* **2004**, 749–760; b) D. A. Keen, *Crystallogr. Rev.* **2020**, *26*, 143–201.
- [4] a) M. Juelsholt, T. Lindahl Christiansen, K. M. Ø Jensen, *J. Phys. Chem. C* **2019**, *123*, 5110–5119; b) F. C. Firth, M. W. Gaultois, Y. Wu, J. M. Stratford, D. S. Keeble, C. P. Grey, M. J. Cliffe, *J. Am. Chem. Soc.* **2021**, *143*, 19668–19683.
- [5] L. Yang, P. Juhas, M. W. Terban, M. G. Tucker, S. J. L. Billinge, *Acta Crystallogr. Sect. A* **2020**, *76*, 395–409.
- [6] S. Banerjee, C.-H. Liu, K. M. O. Jensen, P. Juhas, J. D. Lee, M. Tofanelli, C. J. Ackerson, C. B. Murray, S. J. L. Billinge, *Acta Crystallogr. Sect. A* **2020**, *76*, 24–31.
- [7] a) Z. Thatcher, C.-H. Liu, L. Yang, B. C. McBride, G. Thinh Tran, A. Wustrow, M. A. Karlsen, J. R. Neilson, D. B. Ravnsbæk, S. J. Billinge, *Acta Crystallogr. Sect. A* **2022**, *78*; b) C.-H. Liu, C. J. Wright, R. Gu, S. Bandi, A. Wustrow, P. K. Todd, D. O’Nolan, M. L. Beauvais, J. R. Neilson, P. J. Chupas, *J. Appl. Crystallogr.* **2021**, *54*.
- [8] a) J. Buha, D. Arçon, M. Niederberger, I. Djerdj, *Phys. Chem. Chem. Phys.* **2010**, *12*, 15537–15543; b) G. Garnweitner, M. Niederberger, *J. Am. Ceram. Soc.* **2006**, *89*, 1801–1808; c) M. Niederberger, G. Garnweitner, *Chem. Eur. J.* **2006**, *12*, 7282–7302.
- [9] a) K. J. Griffith, K. M. Wiaderek, G. Cibin, L. E. Marbella, C. P. Grey, *Nature* **2018**, *559*, 556–563; b) K. J. Griffith, A. C. Forse, J. M. Griffin, C. P. Grey, *J. Am. Chem. Soc.* **2016**, *138*, 8888–8899; c) A. Llordés, Y. Wang, A. Fernandez-Martinez, P. Xiao, T. Lee, A. Poulain, O. Zandi, C. A. Saez Cabezas, G. Henkelman, D. J. Milliron, *Nat. Mater.* **2016**, *15*, 1267–1273; d) G. Cai, R. Zhu, S. Liu, J. Wang, C. Wei, K. J. Griffith, Y. Jia, P. S. Lee, *Adv. Energy Mater.* **2022**, *12*, 2103106; e) H. C. Lu, S. Ghosh, N. Katyal, V. S. Lakhanpal, I. R. Gearba-Dolocan, G. Henkelman, D. J. Milliron, *ACS Nano* **2020**, *14*, 10068–10082.
- [10] a) H. Zheng, J. Z. Ou, M. S. Strano, R. B. Kaner, A. Mitchell, K. Kalantar-zadeh, *Adv. Funct. Mater.* **2011**, *21*, 2175–2196; b) J. W. J. Wu, R. Moriyama, M. Nakano, K. Ohshimo, F. Misaizu, *Phys. Chem. Chem. Phys.* **2017**, *19*, 24903–24914; c) H. Schafer, R. Gruehn, F. Schulte, *Angew. Chem. Int. Ed.* **1966**, *5*, 40–52; *Angew. Chem.* **1966**, *78*, 28–41.
- [11] a) A. Magneli, *Acta Crystallogr.* **1953**, *6*, 495–500; b) S. Iijima, J. G. Allpress, *Acta Crystallogr. Sect. A* **1974**, *A 30*, 22–30.
- [12] a) M. Juelsholt, A. S. Anker, T. L. Christiansen, M. R. V. Jørgensen, I. Kantor, D. R. Sørensen, K. M. Ø Jensen, *Nanoscale* **2021**, *13*, 20144–20156; b) T. L. Christiansen, E. D. Bøjesen, M. Juelsholt, J. Etheridge, K. M. Ø Jensen, *ACS Nano* **2019**, *13*, 8725–8735; c) O. Aalling-Frederiksen, M. Juelsholt, A. S. Anker, K. M. Ø Jensen, *Nanoscale* **2021**, *13*, 8087–8097.
- [13] S. Andersson, A. D. Wadsley, *Nature* **1966**, *211*, 581–583.
- [14] C. Nico, T. Monteiro, M. P. Graça, *Prog. Mater. Sci.* **2016**, *80*, 1–37.
- [15] J. L. Myers, A. Well, R. F. Lorch, *Research Design and Statistical Analysis*, Routledge, **2010**.
- [16] a) A. F. Sapnik, I. Bechis, A. M. Bumstead, T. Johnson, P. A. Chater, D. A. Keen, K. E. Jelfs, T. D. Bennett, *Nat. Commun.* **2022**, *13*, 2173; b) K. T. Mukaddem, P. A. Chater, L. R. Devereux, O. K. Al Bahri, A. Jain, J. M. Cole, *J. Phys. Chem. C* **2020**, *124*, 11935–11945; c) K. T. Mukaddem, J. M. Cole, K. A. Beyer, S. O. Sylvester, *J. Phys. Chem. C* **2020**, *124*, 10094–10104; d) P. Bordet, *C. R. Phys.* **2018**, *19*, 561–574.
- [17] D. O’Nolan, H. Zhao, Z. Chen, A. Grenier, M. L. Beauvais, M. A. Newton, T. M. Nenoff, P. J. Chupas, K. W. Chapman, *Chem. Sci.* **2021**, *12*, 13836–13847.
- [18] a) M. W. Terban, S. J. L. Billinge, *Chem. Rev.* **2022**, *122*, 1208–1272; b) S. Habermehl, C. Schlesinger, D. Prill, *J. Appl. Crystallogr.* **2021**, *54*, 612–623; c) T. Davis, M. Johnson, S. J. L. Billinge, *Cryst. Growth Des.* **2013**, *13*, 4239–4244.
- [19] L. Yang, E. A. Culbertson, N. K. Thomas, H. T. Vuong, E. T. Kjaer, K. Jensen, M. G. Tucker, S. J. Billinge, *Acta Crystallogr. Sect. A* **2021**, *77*, 2–6.
- [20] J. Becker, M. Bremholm, C. Tyrsted, B. Pauw, K. M. Ø Jensen, J. Eltzholt, M. Christensen, B. B. Iversen, *J. Appl. Crystallogr.* **2010**, *43*, 729–736.
- [21] P. J. Chupas, X. Qiu, J. C. Hanson, P. L. Lee, C. P. Grey, S. J. L. Billinge, *J. Appl. Crystallogr.* **2003**, *36*, 1342–1347.
- [22] G. Ashiotis, A. Deschildre, Z. Nawaz, J. P. Wright, D. Karkoulis, F. E. Picca, J. Kieffer, *J. Appl. Crystallogr.* **2015**, *48*, 510–519.
- [23] P. Juhas, T. Davis, C. L. Farrow, S. J. L. Billinge, *J. Appl. Crystallogr.* **2013**, *46*, 560–566.
- [24] P. Virtanen, R. Gommers, T. E. Oliphant, M. Haberland, T. Reddy, D. Cournapeau, E. Burovski, P. Peterson, W. Weckesser, J. Bright, S. J. van der Walt, M. Brett, J. Wilson, K. J. Millman, N. Mayorov, A. R. J. Nelson, E. Jones, R. Kern, E. Larson, C. J. Carey, Í. Polat, Y. Feng, E. W. Moore, J. van der Plas, D. Laxalde, J. Perktold, R. Cimrman, I. Henriksen, E. A. Quintero, C. R. Harris, A. M. Archibald, A. H. Ribeiro, F. Pedregosa, P. van Mulbregt, A. Vijaykumar, A. P. Bardelli, A. Rothberg, A. Hilboll, A. Kloeckner, A. Scopatz, A. Lee, A. Rokem, C. N. Woods, C. Fulton, C. Masson, C. Häggström, C. Fitzgerald, D. A. Nicholson, D. R. Hagen, D. V. Pasechnik, E. Olivetti, E. Martin, E. Wieser, F. Silva, F. Lenders, F. Wilhelm, G. Young, G. A. Price, G.-L. Ingold, G. E. Allen, G. R. Lee, H. Audren, I. Probst, J. P. Dietrich, J. Silterra, J. T. Webber, J. Slavič, J. Nothman, J. Buchner, J. Kulick, J. L. Schönberger, J. V. de Miranda Cardoso, J. Reimer, J. Harrington, J. L. C. Rodríguez, J. Nunez-Iglesias, J. Kuczynski, K. Tritz, M. Thoma, M. Newville, M. Kümmerer, M. Bolingbroke, M. Tartre, M. Pak, N. J. Smith, N. Nowaczyk, N. Shebanov, O. Pavlyk, P. A. Brodtkorb, P. Lee, R. T. McGibbon, R. Feldbauer, S. Lewis, S. Tygier, S. Sievert, S. Vigna, S. Peterson, S. More, T. Pudlik, T. Oshima, et al., *Nat. Methods.* **2020**, *17*, 261–272.
- [25] S. Gražulis, D. Chateigner, R. T. Downs, A. Yokochi, M. Quirós, L. Lutterotti, E. Manakova, J. Butkus, P. Moeck, A. Le Bail, *J. Appl. Crystallogr.* **2009**, *42*, 726–729.
- [26] G. Bergerhoff, R. Hundt, R. Sievers, I. Brown, *J. Chem. Inf. Comput. Sci.* **1983**, *23*, 66–69.
- [27] P. Juhas, C. L. Farrow, X. Yang, K. R. Knox, S. J. L. Billinge, *Acta Crystallogr. Sect. A* **2015**, *71*, 562–568.
- [28] C. L. Farrow, P. Juhas, J. W. Liu, D. Bryndin, E. S. Božin, J. Bloch, T. Proffen, S. J. L. Billinge, *J. Phys. Condens. Matter* **2007**, *19*, 335219.
- [29] L. Yang, E. A. Culbertson, N. K. Thomas, H. T. Vuong, E. T. S. Kjaer, K. M. O. Jensen, M. G. Tucker, S. J. L. Billinge, *Acta Crystallogr. Sect. A* **2021**, *77*, 2–6.

- [30] T. L. Christiansen, S. R. Cooper, K. M. Ø Jensen, *Nanoscale Adv.* **2020**, *2*, 2234–2254.
- [31] M. Niederberger, M. H. Bartl, G. D. Stucky, *J. Am. Chem. Soc.* **2002**, *124*, 13642–13643.
- [32] Z. Zhao, Y. Bai, W. Ning, J. Fan, Z. Gu, H. Chang, S. Yin, *Appl. Surf. Sci.* **2019**, *471*, 537–544.
- [33] a) O. C. Gagné, F. C. Hawthorne, *IUCrJ* **2020**, *7*, 581–629; b) F. Tamadon, K. Seppelt, *Angew. Chem. Int. Ed.* **2013**, *52*, 767–769; *Angew. Chem.* **2013**, *125*, 797–799.
- [34] M. T. Pope, A. Muller, *Angew. Chem. Int. Ed.* **1991**, *30*, 34–48; *Angew. Chem.* **1991**, *103*, 56–70.
- [35] P. Debye, *Annalen der Physik* **1915**, *351*, 809–823.
- [36] I. Olliges-Stadler, J. Stötzler, D. Koziej, M. D. Rossell, J. D. Grunwaldt, M. Nachtegaal, R. Frahm, M. Niederberger, *Chem. Eur. J.* **2012**, *18*, 2305–2312.

Manuscript received: April 30, 2022
Version of record online: August 3, 2022